Journal of Ship Research, Vol. 39, No. 3, Sept. 1995, pp. 202–212

Propeller Blade Cavitation Inception Prediction and Problems of Blade Geometry Optimization: Recent Research at the Krylov Shipbuilding Research Institute

E. L. Amromin,[1] **A. V. Vasiliev,**[1] and **E. N. Syrkin**[1]

An analytical method for cavitation inception number predictions that is applicable also to blade geometry optimization is described. Test and numerical data on full-scale propellers operating near the ship hull are given along with model results from cavitation tunnel tests. The paper may be regarded as a general review of research carried out and partially published in Russia during the past decade.

Introduction

A TRADITIONAL long-time requirement in propeller design has been to achieve appropriate blade cavitation characteristics. The need to reduce propeller-induced noise and vibrations stimulated research on cavitation inception as early as the 1950s.

Propeller cavitation may manifest itself in various forms under different inception conditions and with different consequences. The incipient forms are highly susceptible to scale effects that cause major difficulties in laboratory testing in regard to establishing a correlation between model data and full-scale measurements. Numerical techniques also have their limitations in cavitation inception prediction due to the difficulty of computing blade pressures, even without the cavitation, and because of the lack of an adequate theoretical understanding of incipient cavitation.

Therefore, the most common routine has been to apply a semi-empirical method to translate model results into full-scale values with the help of certain relations: "the scale extrapolators." This was done assuming that the cavitation inception number was related to the Reynolds number as $\sigma_i \sim \mathrm{Rn}^m$, with m being dependent on the form of the cavitation but not on the blade geometry. The m-values were selected from experimental data suggested by Billet & Holl (1979) among others.

In addition, it was also assumed that with the same advance ratios $J = V_x/nD$ the model and the full-scale propellers would have the same form of cavitation, and it was thought allowable to use a quasi-steady approach to cavitation prediction. Thus, σ_i would be determined assuming the propeller was operating in a steady uniform flow with the velocity equal to the extreme instantaneous values V_x of the unsteady inflow. The latter assumption has enabled use of uniform flow tunnel results to predict cavitation inception by plotting model $\sigma_i(J)$ curves from acoustic or visual data. The range of J variations was normally taken according to the range of propeller disk velocities from towing tank or cavitation tunnel measurements.

Aiming at maximum efficiency, the designers tended to choose Betz's optimum radius-wise circulation distributions. Such propellers had large load gradients on their blade tips and, therefore, produced strong tip vortices. Their models showed cavitation at relatively high cavitation numbers. The vortex cavitation was attributed the maximum scale extrapolator and was considered to be the most dangerous form. For this reason the main design efforts were directed at reducing the tip vortex intensity, which was achieved by (*a*) increasing the number of blades and (*b*) unloading the blade tip sections. Additionally, some special measures were taken to reduce inflow nonuniformity at the top part of the blade.

Such propeller design techniques have been used in Russia since the mid-60s and as a result the vortex cavitation inception numbers by late 1970s were reduced by three to four times. Model tests were indicating that even with such designs the tip vortex cavitation still preceded all other forms of blade cavitation.

In the early 1980s a project was staged to make full-scale observations on high-speed ships. It covered six propellers with identical blade planes, load distributions, and blade section profiles. The inflow parameters, in particular the values of $(V_{max} - V_{min})/V_p$, were also almost identical. The only difference in trial conditions was in the unit hydrodynamic loads. The relevant propeller geometry data may be found in Table 1. The skew angle was 30 deg, the disk area A_0/A_e = 1.15, and the blade section was close to the NACA-66 profile but with slightly sharper leading edges.

In Table 1, f_{max} and t_{max} are the dimensionless curvature and thickness of the blade section, r is the relative radius, and D the propeller diameter.

The full-scale observations revealed no expected tip vortex cavitation on propellers with unloaded tips. When the tip vortex cavitation nevertheless started, it was at speeds much higher than predicted by scaling the model test data.

At the same time, suction side sheet cavitation near the blade leading edges was observed to be the dominating form of cavitation under full-scale conditions, although it has never been reported when testing 200-mm-diameter (~8 in.) models.

It was found that cavity distribution along the radius significantly depended on the propeller's unit hydrodynamic load. At thrust-load coefficients of C_τ = 0.35–0.4 observers have noted first flashes of cavitation at r = 0.9–0.95 and with C_τ increased to 0.6–0.7 the cavities started appearing at r = 0.6–0.7 (Fig. 1). The relevant velocity distribution from towing tank measurements is shown in Fig. 2.

Thus, full-scale observations disclosed that the traditional semi-empirical approach was not applicable for propellers with improved cavitation performance, that the adopted assumptions were invalid, and that the forms of cavitation on

[1]Krylov Shipbuilding Research Institute, St. Petersburg, Russia.

Manuscript received at SNAME headquarters October 16, 1992; revised manuscript received May 5, 1993.

Table 1 Propeller geometry parameters

r	0.25	0.3	0.4	0.5	0.6	0.7	0.8	0.9	0.95	1
P/P (0.7)	1.130	1.12	1.100	1.067	1.04	1.0	0.933	0.893	0.747	0.620
$2f_{max}/D$	0.0072	0.0110	0.0168	0.0189	0.0181	0.0156	0.0125	0.0070	0.0033	0
$2t_{max}/D$	0.078	0.072	0.0585	0.0490	0.0430	0.0390	0.0364	0.035	0.0324	0

model and realistic propellers were quite different. This convinced the researchers that model cavitation tests were a doubtful tool for blade optimization and that new efforts should be made to find a correct computational technique to predict full-scale incipient sheet cavitation.

Fortunately, by the 1980s the grounds for developing such methods were available.

First, the numerical methods for blade pressure distributions without cavitation offered by Greely & Kerwin (1982) and Bavin et al (1983) have already been sufficiently well established.

Second, the experimental studies on incipient forms of cavitation for bodies of revolution carried out by Arakeri (1975) and Arakeri & Acosta (1976) have shown a deeper physical understanding of the phenomenon. This allowed Amromin (1985,1988) to develop a method for computing partial cavitation based on the two-dimensional viscous separation theory offered by Gogish & Stepanov (1982) and Ivanov's (1983) method for jet problems in ideal fluid.

Since a method to calculate full-scale σ_i was made available, it became possible to optimize propeller blades based on performance predictions for cavitating propellers behind ship hulls.

The method is described briefly in the following together with a discussion on its practical applicability to σ_i computations, including a comparison of numerical results with full-scale propeller measurements.

Review of viscous fluid cavitation theory; method for sheet cavitation numerical prediction

Until recently the cavitation inception number was found theoretically, assuming that cavities were negligibly small in respect of σ_i. This assumption was implicitly or explicitly present in many attempts to predict σ_i through the isolated bubble evolution in a known pressure field or to study pressure distribution and fluctuations prior to the onset of cavitation. Such attempts have inevitably failed to reach a satisfactory agreement with experimental data.

The fact is that though cavitation numbers close to σ_i, cavity dimensions are really small compared with the length and diameter of the involved body, the cavity thickness turns out to be of the same order as that of the boundary layer. Therefore, even a tiny cavity is capable of sizably affecting pressure distribution within the nearby part of the body surface.

The authors have derived a way to account for these changes induced by cavity-to-boundary layer interactions. This technique for computing σ_i involves a concept long used for the purpose in experimental studies: selecting the maximum cavitation number σ_i from a test series with decreasing velocity or increasing pressure of the inflow. The authors realize that this actually gives them the cavitation cessation number, but when the wake air content is not too high this number normally differs from σ_i only slightly. This difference was experimentally studied by van Meulen (1980) and the same concept was advocated by Huang & Peterson (1976) in their calculations. However, the latter exercise was not exactly accurate in accounting for the interaction between cavities and the boundary layer and was based on the theory described by Gourevitch (1970) with the cavity inception position being removed. Gourevitch's dependence on the position of cavitation inception versus the laminar-turbulent transition in the body's boundary layer lacks strong substantiation and there are many contradictory experimental results.

Gorshkov & Kalashnikov (1970), for example, have observed cavitation inception on a 16th caliber body of revolution only long after the transition, while van Meulen (1980) reported it to occur much earlier than the transition. Experimental results obtained by Arakeri & Acosta (1976) speak directly against the idea of this dependence; they've had a situation when a turbulence stimulator provoked earlier transition but suppressed the cavitation inception.

To illustrate the major points of our new theory a corresponding flow scheme is shown in Fig. 3. It will be further used for comparison with the famous theory of "ideal cavitation" (in Birkhoff's terminology).

The authors resolve the cavitation problem through the concept of viscous-potential interaction according to which the flow is divided into a potential flow zone and a boundary layer with their separating margin being unknown. In the new theory the cavity and the potential flow margins are separated by the boundary layer. Under the ideal cavitation theory these boundaries coincide.

According to the ideal cavitation theory, the cavity boundary merges smoothly with the body's outline always remaining normal to it. The authors take into account the fact that due to the capillarity in real fluid there is a certain angle β between the cavity margin and the surface of the body placed in the flow (Fig. 3). This β-angle depends on the body's wettability.

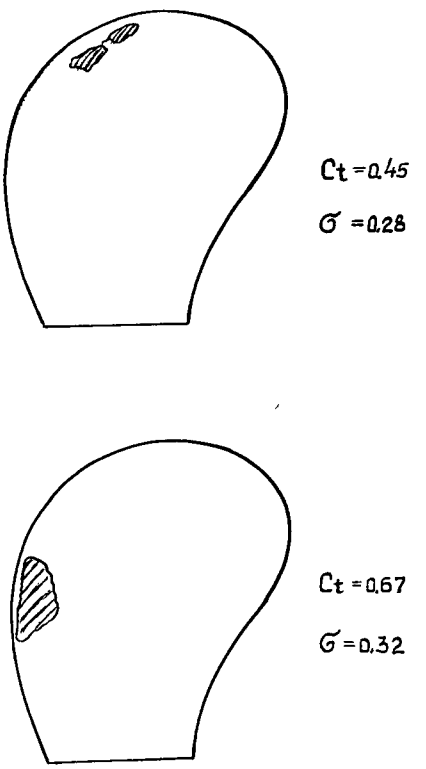

Fig. 1 Forms of cavities on full-scale propellers blades

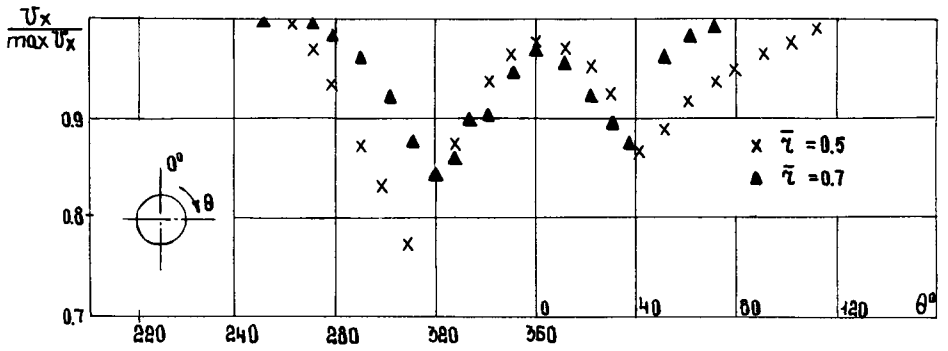

Fig. 2 Axial velocity distribution from towing tank model measurements

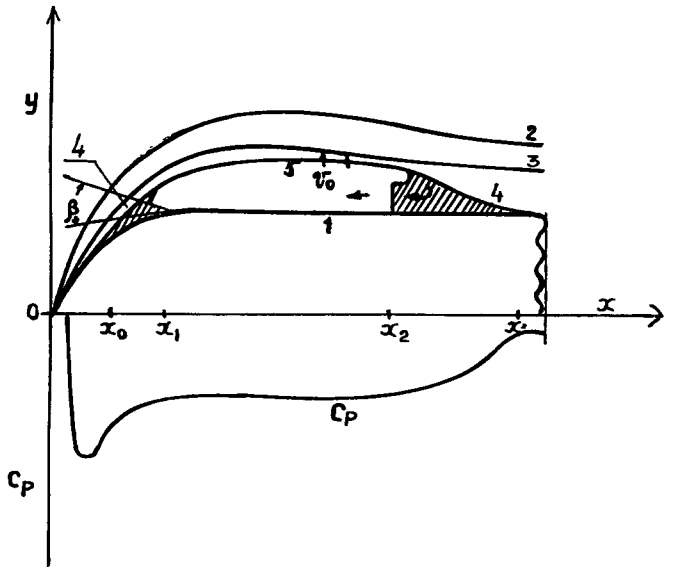

1. section of flowing body
2. boundary layer border
3. displacement body boundary
4. back-flow zone
5. cavity boundary

Fig. 3 Cavitation flow on viscous and capillar fluid. Arrows show direction of fluid transfer through cavity boundary

The β-effect in displacing the cavity starting point was established by Ivanov (1980) during his experiments with an ellipsoid of revolution assembled from two parts of different materials. For the Teflon℠ (trifluoroethylene) part he found $\beta = \pi/2$; for the aluminium one it was $\beta \simeq 0$. The difference in β-angles resulted in shifting the cavity starting point for more than 0.1 of the ellipsoid's diameter. Amromin (1993) published the relevant computations in his first paper on this subject describing some of the early results made jointly with Ivanov in 1982 in the "Doklady" of the USSR Academy of Sciences.

With the kind of attachment of boundaries explained in the foregoing, a viscous separation zone is formed in front of the cavity. This was demonstrated experimentally by Arakeri (1975); the zone is shaded in Fig. 3.

In ideal cavitation the cavity boundary is completed by an imaginary body (e.g., under Riabushinsky's scheme) or backstreams which carry the fluid out of the flow plane. The new scheme also contains a backflow stream which causes another separation zone (also shaded in Fig. 3). However, in this theory the fluid travels across the cavity boundary and into its boundary layer like that shown by an arrow in the scheme.

The ideal cavitation theory assumes that the potential-flow coefficient remains constant anywhere along the cavity boundary: $Cp = -\sigma$. Approximate Cp values computed according to the new concept are shown in Fig. 3. There the $Cp(x)$-function has two zones with increasing pressures at the cavity ends and a practically isobaric area at the mid-part of the cavity boundary, that is:

$$Cp = \begin{cases} C_1(x - x_1 - \epsilon)^2 - \sigma & \text{for } x_0 \leqslant x \leqslant x_1 + \epsilon \\ -\sigma & \text{for } x_1 + \epsilon < x < x_2 \\ C_2(x - x_2)^2 - \sigma & \text{for } x_2 \leqslant x \leqslant x_3 \end{cases}$$

where the $\epsilon \ll x_2 - x_1$ distance here is initially unknown. Naturally, among the first priorities is to find numbers C_1, C_2, as well as the x_0 and x_3 longitudinal coordinates of the front and aft points of the separation zone. An unknown value within this zone is h—the distance between the body and the potential-flow S margin. The condition relevant for it is

$$Cp = 1 - (\nabla\Phi, \nabla\Phi) = F(x, C_1, C_2, x_0, x_1, x_2, x_3) \qquad (1)$$

To compute h it is necessary to apply a boundary condition of zero normal velocity for a displacement body in $[x_0, x_3]$. This requires distributing intensity sources on the body's surface. The $q(x)$-function is found from the above condition (1) using the singular equation theory described in Newman's book (1977). Then h may be obtained from:

$$q = 2\frac{d(hU^*)}{dl} \qquad (2)$$

where l is the arc length and U^* the potential cavitation-free flow velocity on the surface of the body.

Y can be found with the help of the Laplace formula:

$$Cp + \sigma = 2\kappa \mathrm{We}^{-1} \qquad (3)$$

The Weber number (We) is generated according to the typical body size C. The cavity boundary curvature κ contains the second derivative of Y. Therefore, (3) is an ordinary second-order differential equation for Y, and to compute Y two conditions should be satisfied at the $x = x_1$ point:

$$Y = y_1; \quad \frac{dY}{dl} = -\operatorname{tg}(\beta) \qquad (4),(5)$$

However, to establish Cp and to calculate q from (1), it is necessary to have six parameters $\{C_1, C_2, x_0, x_1, x_2, x_3\}$. It is more convenient to assume $\{\sigma, \mathrm{We}\}$ unknown and to assign a couple of numbers $\{x_1, x_2\}$, but anyway six conditions would be needed to determine the six parameters. The following conditions are chosen for this purpose.

- The condition of viscous-potential interaction:

$$\delta^*(x_3) = h(x_3) \qquad (6)$$

- The condition of the boundary-layer attachment to the cavity at a distance ϵ from the stream separation point:

$$Y(x_1 + \epsilon) = h\,(x_1 + \epsilon) - \delta^*(x_1 + \epsilon) \tag{7}$$

- Local conditions of the boundary-layer separation and reattachment before and after the cavity:

$$x_1 - x_0 = 60 \left| \frac{\delta}{C} \right|^{\frac{5}{7}} \left| \frac{C}{ReU} \frac{dU}{dl} \right|^{\frac{1}{7}} \left| 1.1 + \frac{\delta^{*2} Re}{UC} \frac{dU}{dl} \right|^{-\frac{3}{7}} \tag{8}$$

$$12[B - \delta^*(x_3)]^{1.25}[\delta^*(x_2 + \epsilon_1)]^{0.25} = (x_3 - x_2)(x_2 - x_1 - \epsilon)^{0.5} \tag{9}$$

where δ^* is the displacement thickness, B the maximum cavity thickness, $U = -\partial\Phi/\partial l$, $L = x_2 - x_1$, and $\epsilon_1 \to 0$. The continuity condition at the x-point:

$$\partial U/\partial l(x_0 + \epsilon_1) = \partial U/\partial l(x_0 - \epsilon_1) \tag{10}$$

- The f_3 of q limitation anywhere within $[x_0, x_3]$:

$$\int_{x_0}^{\alpha_3} \frac{f_3(x)dx}{\sqrt{(x - x_0)(x_3 - x)}} = 0 \tag{11}$$

The rule for generating the $f(x)$ function in equations similar to (1) has been explained by Newman (1977).

The above conditions (7)–(9) contain a new unknown function δ^*. This may be found from the Karman equation written for the cavity boundary as

$$\frac{d\delta^{**}}{dl} + \frac{dU}{dl}\frac{(2\delta^{**} + \delta^*)}{U} + \frac{V_0}{U}\left(1 - \frac{u_0}{U}\right) = 0 \tag{12}$$

The authors suppose $V_0(x) = V_1[(x - x_1 - \epsilon)/(x_2 - x_1 - \epsilon)]^p$, where v_1 is an unknown constant. Amromin (1985) has shown the influence of p upon $L(\sigma)$ to be weak and, therefore, it is possible to assume $p = 1$.

The cavity boundary friction is negligible but the velocity components $\{u_0, v_0\}$ here are not equal to zero. There are four unknown functions in (12), but assuming a velocity profile of a relevant wake type it is possible to express δ^{**} through δ^* and u_0/U.

Amromin (1985) found that the $v(x)$ distribution produced only a slight effect upon the cavity configuration while the total flow rate through the cavity side surface corresponded to the time-average quantity of the fluid brought by the backflow stream.

To compute U it is possible to apply Prandtl's equation for the zero function line:

$$u_0 \frac{du_0}{dl} = K_1 \frac{(U - u_0)^3}{U\,\delta^*} + U\frac{dU}{dl} \tag{13}$$

where K_1 is constant.

The inputs required for (12) are taken from the body boundary-layer calculations for the upstream from the cavity region. That may be done utilizing any of the existing methods.

Thus, equations (1)–(3), (12), and (13) for functions $\{u_0, \delta^*, Y, q, h\}$ with eight supplementary conditions (4)–(11) for parameters $\{v_1, x_0, \epsilon, x_3, C_1, C_2, \sigma, We\}$ are sufficient to solve viscous cavitation problems. A more detailed description of the computation procedure may be found in the earlier mentioned paper by Amromin, Vasiljev, and Droblenkov.

The new theory also permits us to involve more input data. It is now possible to account not only for σ but for the values β, Rn, We and the inflow turbulence as well. It is possible to find C-values and $V\infty$ inflow velocities for each pair of {Rn,We} corresponding to the same σ-values. The computation procedure for this theory was thoroughly described by Amromin (1993).

Maybe some time in the future there will be as many schemes available for the viscous streams in the cavity afterpart as there are now in the ideal fluid stream theory. However, we don't yet have them. Neither do we have information about utilizing any computation procedure for partial cavitation, e.g., the scheme offered by Tulin & Hsu (1980).

Therefore, the authors will now attempt to compare their numerical results with the available experimental data. The correlation between the computations carried out under the new concept and test data is described below.

The data related to cavity location on a body of revolution with a hemisphere-shaped bow part may be seen in Fig. 4. The experimental results for this most simple and popular configuration are available in many papers, starting with the one by Knapp, Daily, & Hammit (1970). However, all data refer to Rn = 6.10^5 and 2-in.-diameter models.

The ideal cavitation theory (Fig. 4, dashed line) greatly overestimates the cavity dimensions with the increase in σ, thus sizably overestimating σ_i = max σ. When the cavity length L is sufficiently large, the ideal cavitation theory predictions are rather accurate but still worse than those provided by the new theory. All these calculations were made for $\beta = 0$, which corresponds to metallic bodies. Comparing the ideal cavitation analytical predictions with test data of an 8% wing profile, one may observe a stronger discrepancy in the cavity after-edge longitudinal position $x_2(\sigma)$.

In this example the situation is complicated by the lifting force and the sharp change of pressure on a small part of the body. Experimental results from Yamaguchi & Kato (1983) are shown in Fig. 5, which indicates the scatter in measurements. The success of the new theory in establishing x_2 comes largely thanks to the ability to account for the Rn effects upon the profile's Cy. To compute the Cy(Rn, α)-function the authors use an analytical approximation of wing profile calculations originally suggested by Mishkevitch and published later by Mishkevitch, Amromin, & Rozhdestvensky (1990).

Such an advance in cavitation calculations for bodies in viscous flow holds promise for achieving satisfactory results in σ_i predictions. The $\sigma(L)$ function shown in Fig. 6 corresponds to partial cavitation calculations for propeller blade cylinder sections. It may be seen that σ_i was achieved by $L > 0$ due to capillary effects. For a thin profile with a not very high value of Cy the σ maximum would come at an L-value too small for visualization. This may be a possible cause of errors in experiments and underestimations in σ_i predictions.

For the hemispheric-bow bodies of revolution the minimum L-values are considerably larger and the $Cp(l)$ plots become smoother. This allows us to assume that Fig. 7 shows a quite correct comparison between such analytical results and the

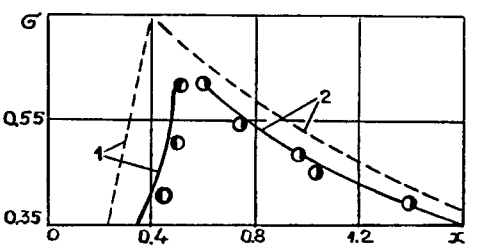

◐◑ experimental data
dashed line ideal fluid calculations
solid line viscous fluid calculations
1. cavity fore line
2. cavity aft line

Fig. 4 Cavity location on a hemispherical bow body of revolution

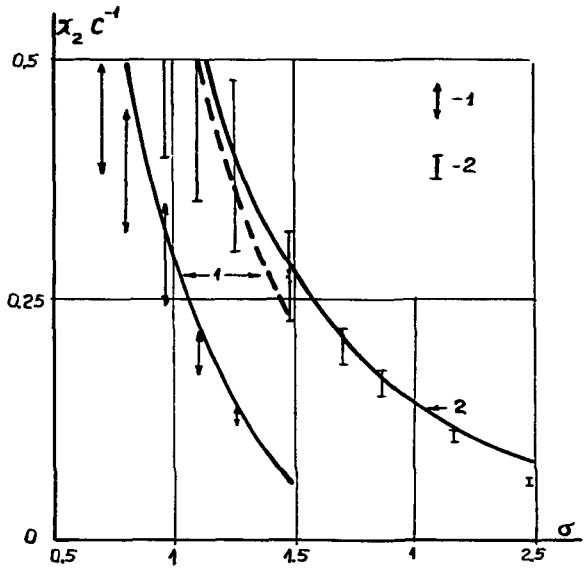

solid line authors' calculation for viscous flow;
dashed line calculation for ideal flow at experimental points. Curve 1 refers to 4 deg, curve 2 to 6 deg

Fig. 5 Comparison of measured and calculated cavity lengths on an 8% profile

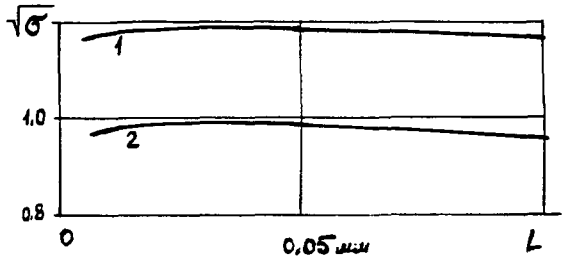

Fig. 6 Cavitation number function versus cavity length on blade profiles. Curves 1 and 2 correspond to different angles of attack; blade section profile is described in Table 2

measurements reported by Gorshkov & Kalashnikov (1970) and Arakeri & Acosta (1976). Arakeri & Acosta have given a satisfactory theoretical description of their experimental results with a turbulence stimulator. The paradoxical disappearance of cavitation with increasing V_∞ at C = const was explained by the influence of the boundary-layer flow regime upon the conditions of its separation before the cavity and the cavity's equilibrium. There have been sharp changes in the cavity dimensions at just the same Rn because of altering the above-mentioned conditions by introducing a turbulence stimulator: In a turbulent boundary layer the cavities are shifted into the domain of larger dCp/dl and smaller suction values.

Practical applicability for incipient blade cavitation calculations

It is important to emphasize that the aforementioned numerical cavitation predictions for two-dimensional axisymmetric steady flows have been achieved largely due to the sufficiently accurate computation procedure for Cp at fixed potential flow boundaries. Certain aspects make it more difficult to reach similar accuracy in propeller blade Cp calculations, among them: sophisticated blade geometry requiring a huge computer capacity for precise calculations, viscosity effects on blade load distribution, nonuniform inflow causing unsteady flow around the blades, cavitation effects upon

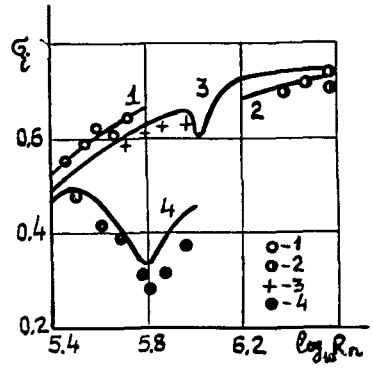

1. C = 0.02 m
2. C = 0.40 m
3. C = 0.05 m
4. C = 0.05 m

Fig. 7 Function σ, (Rn) for a hemispherical bow body for low-air-content wake experiments with turbulence stimulators. Curve numbers correspond to experimental points

blade surface pressure distribution, and direction of streamlines near the edges.

The authors regret their inability to overcome all these difficulties. However, they've managed to escape them insofar as propellers with low cavitation inception numbers are concerned, and the ways to reach this target are described below.

With such propellers during the initial stage of cavitation the cavities remain close to the leading edge at relative radii, yet far from 1, while the cavity thickness is much less than that of the blade at the same radius. Therefore, it is allowable in this problem to suppose that the potential-flow streamlines do not deviate far from the cylinder blade sections and the cavity thickness does not significantly affect the lift of these sections. Under these assumptions the computation of a three-dimensional cavity on the blade may be divided into two parts. First is the calculation of the blade pressure distribution $Cp(x,r)$ in viscous unsteady cavitation free flow, and second is the aggregation of thin two-dimensional cavities on cylinder blade sections with known inflow velocity $U^*(x,r) = (1 - Cp^*(x,r))^{0.5}$, Rn($r$), We($r$), and β and n which are common to the whole blade.

In this second part of the problem

$$Cp(x,r) = Cp^*(x,r) - 2U^*(x,r)\, u(x,r)$$

where $u(x,r)$ is the contribution of sources and sinks simulating the thin cavity and the separation zone computed individually for every section.

The efficiency of such problem division was demonstrated by Amromin, Mishkevitch, & Rozhdestvensky (1990) on the propeller tested by Kuiper (1981). The results are shown in Fig. 8, where the continuous line marks the cavity boundary photographed during the experiment; the dashed line indicates the computed boundary. A sizable discrepancy between tests and predictions at $r \to 1$ may be ignored in σ_i calculations since the cavitation appears here only at r = 0.5–0.8. However, Fig. 8 is for the uniform flow available in hydrodynamic tunnels. To compute pressure distribution on propeller blades in nonuniform flow is another quite difficult task. The methods utilized so far need preliminary hydrodynamic load distribution calculations based on the unsteady vortex lifting-surface theory. The processes involved in propeller operation close to the hull are periodic. This permits us to compute hydrodynamic characteristics with the help of Fourier series, though the actual velocity fields are rather complicated and we are forced to compute a great number of

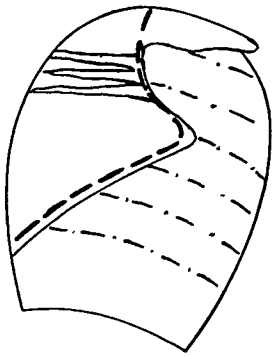

Fig. 8 Comparison of photographed and calculated cavity boundaries on propeller blades

terms for the series. This makes pressure distribution calculations extremely cumbersome. Unsteady nonlinear methods, besides demanding great efforts to generate proper numerical models, call for the use of supercomputers. The latter is necessary in order to cover the vast number of calculation points required to obtain reliable results near the blade edges.

It was found convenient to divide the inflow into two parts: one with high velocity gradients and another with low ones. This opens an opportunity to combine two methods: one the above-described steady-flow technique, and the other a two-dimensional calculation for a profile in a flow gust of an arbitrary shape of the $U(t)$-function. This way it is possible to separate the three-dimensional and the unsteady flow effects. The $Cp^*(x,r)$ calculation is then also split into two tasks.

The first task is to compute blade pressures at given Rn and the advance ratio J in uniform inflow. This is done by an approximate method based on the following concepts. The pressure near a blade or foil-rounded leading edge may be computed by the method of Cole (1968), that is, joining of asymptotic analytical solutions for the edge vicinities with the linear theory results for the mid-part of the involved blade or foil. The effects of Rn upon Cp near the edge may be covered within the ideal fluid assumptions by the angle-of-attack dependence, that is, by violating the Kutta-Joukowski condition. Figure 9 shows the predictions computed with such a violation against the measurements reported by Yamaguchi et al (1983). The comparison indicates a better agreement within the leading-edge vicinity and a significant influence of Rn upon Cp^* in this region.

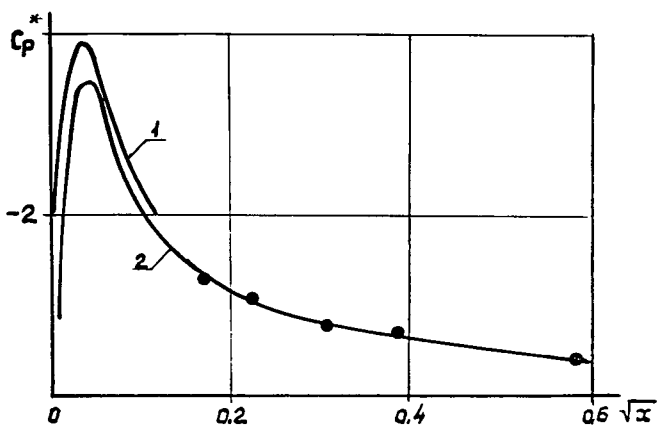

● measurements
1 ideal fluid calculation
2 calculations with Mishkevitch's correction factor

Fig. 9 Influence Rn on pressure distribution for a wing profile

For the second Cp calculation task—the same as in the paper by Amromin, Vasiljev, & Syrkin (1993)—it is assumed that the unsteadiness of the inflow causes only local pressure variations and their contribution may be found with the help of a representative two-dimensional profile concept. Since the most difficult part of this problem is to precisely compute C_p^* close to the maximum suction points, the authors maintain the same cylinder blade section geometry as before. In the formula for the Φ potential of the flow arriving at these sections:

$$\Phi = \Phi_1 (t, x, y) - x + ay + bxy \tag{14}$$

they take a,b coefficients for each $\{J,r\}$ pair to maintain the same $Cy(r,J)$ and $\min C_p^*(x,r,J)$ as already calculated for the three-dimensional steady flow at $\Phi_1 = 0$. The Φ_1 function describes the inflow unsteadiness related to its nonuniform nature. Figure 10 proves that for the maximum suction point vicinities this two-dimensional theory produces results quite close to those of the three-dimensional concept.

Amromin, Vasiljev, & Simeonitcheva (1991) have tested this numerical procedure against Jorber & Covert's (1982) data. Figure 11 confirms that the analytical solution did not overestimate unsteady flow pressure fluctuations and, therefore, may be used for Cp calculations.

Evaluation of quasi-steady assumption applicability for predictions

The described method for computing propeller blade Cp in uniform inflow has been checked against model tests and full-scale cavitation inception observations. At the same time, the authors studied the applicability of the quasi-

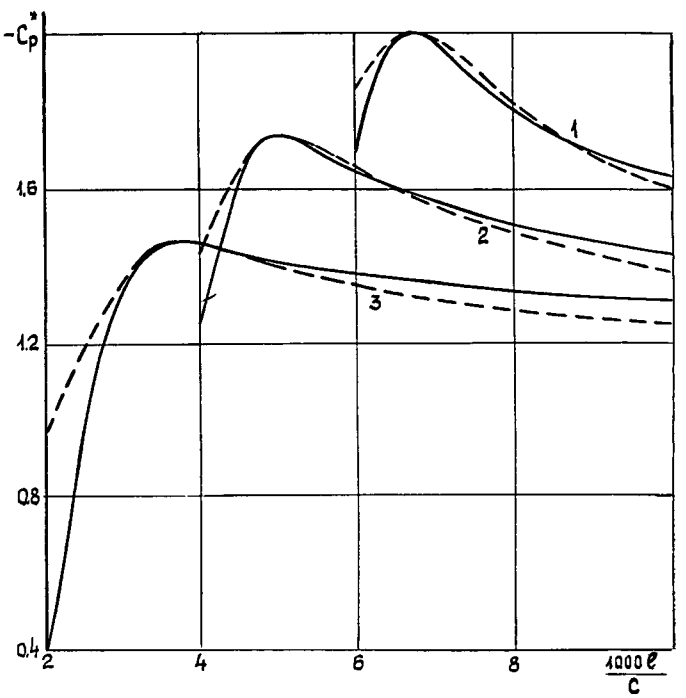

1. $J = 0.51$
2. $J = 0.6$
3. $J = 0.7$

Fig. 10 Comparison of pressure profile on blade sections in uniform 3D flow (dashed line) and in "equivalent" (according to $\{\min Cp, Cy\}$ value) 2D flow (solid line)

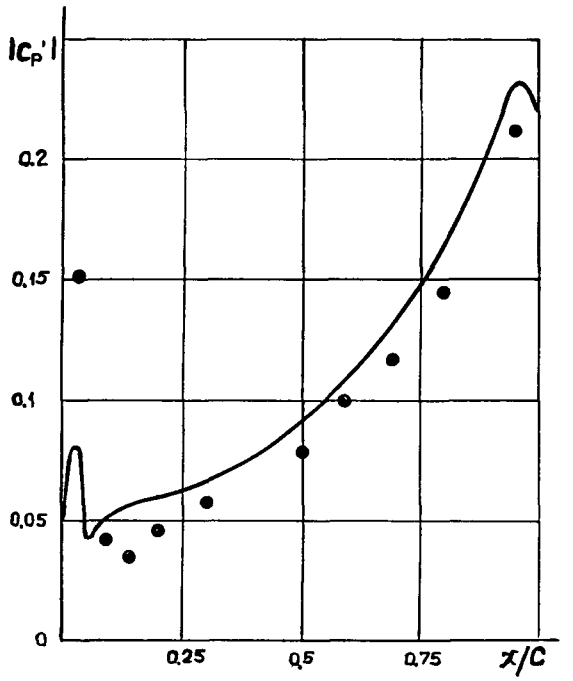

Fig. 11 Comparison of measured and calculated foil pressure fluctuation amplitudes in unsteady flow

steady approach to the problem described here in order to define the conditions which make it necessary to involve the unsteady flow effects in critical cavitation number evaluations and blade optimization.

As mentioned above, sheet cavitation has never been observed on 200-mm-diameter (~8 in.) models. Some tests were staged at the Krylov Institute in the large cavitation tunnel with models of 350 and 400 mm (~14 and 16 in.). Then sheet cavitation was achieved but only at rather small advance ratios, i.e., at high loads (see Fig. 12) when the linear theory errors in Cp predictions are already quite sizable.

Computations to test the comparison show that the new theory is in good qualitative agreement with experimental results for the reason that it correctly reflects tendencies of changes in the cavitation diagram plotted in terms of $\{\sigma_i^{0,5}, J\}$. The traditional semi-empirical cavitation prediction method has already failed to do that.

The ability to account for viscous and capillary effects produces improved quantitative agreement between the analytical and experimental results. This may be seen in Fig. 13, which shows Ri values, i.e., the square root of the ratio of critical cavitation number for uniform and nonuniform flows. Here and in the following description the cavitation numbers are referred to the nD product and not to the inflow velocity. The flow nonuniformity in Fig. 14 was caused by the wake left by a foil.

A certain overestimation of Ri compared with observations may be explained by the difficulties in visual detection of very short cavities in a fluctuating flow.

Calculations of σ_i for full-scale blades have revealed limitations of the quasi-steady concept for establishing $\sigma_i(J)$. This part of the discussion relates to the "A" propeller, one of the two described in Fig. 15. The relevant wake distribution for the ship model is shown in Fig. 2.

Figure 16 demonstrates a comparison of the following results: model diagram for uniform flow; its quasi-steady full-scale prediction corresponding to the local instantaneous J computed through $Vx(\theta)$ distribution; predicted full-scale diagram; and full-scale observation.

It may be seen that steady-flow predictions are close enough to the unsteady ones within the left branch of the plot where they belong to the suction-side cavitation. The situation here is not changed even by the above-noted effects of the unsteady flow around the blade shown in Fig. 17. The slower incoming wake zone is here smaller than the blade chord length and the suction peaks are due to the passage of blade leading and trailing edges through this zone. However, the depressurization value on the suction side is in good agreement with the velocity in the zone. The discrepancy in the pressure side predictions is quite high. This may be explained by the unsteady flow effects neglected in cylinder blade section design when the calculations were made for a fixed range of angles of incidence, ignoring the dynamics of their fluctuations due to rotation.

The authors do not have a means of computing the vortex cavitation. In this regard they have analyzed the flow nonuniformity effects on σ_i by testing 200-mm-diameter model propellers with different design circulation distributions along the radius. The first model had Betz's optimum distribution; the second one had unloaded blade tips (other parameters were common to both models: $z = 5$; skew = about 30 deg; $A_0/A_e = 1.15$). The tests were staged in a small cavitation tunnel (diameter = 0.4 m; Rn = $vDr/\nu = 8.7 \cdot 10^5$, air content = about 1.5%). The setup involved a uniform flow and two nonuniform flows: with a smooth gradient of velocities versus the angle of rotation (propeller in oblique flow) and with sharp velocity gradients (a narrow wake zone behind a foil or an appendage).

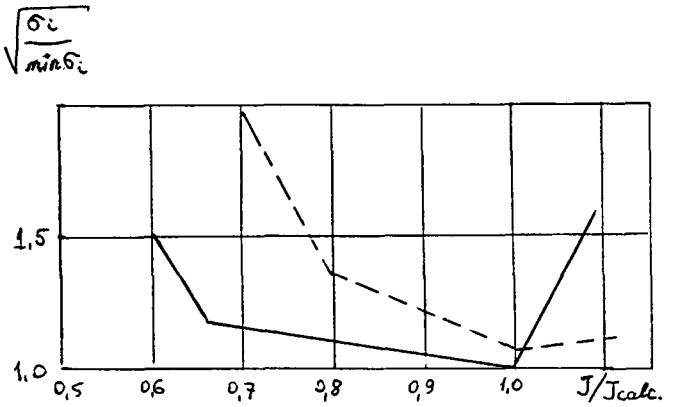

solid line — tip vortex cavitation
dashed line — sheet edge cavitation
J_{calc} — design value of J

Fig. 12 Propeller model cavitation diagram

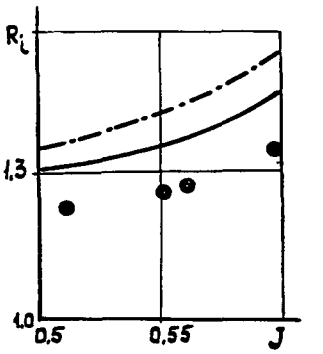

dashed line — ideal flow calculations
solid line — for viscous flow calculations

Fig. 13 Ratio of σ_i in uniform flow and in foil wake

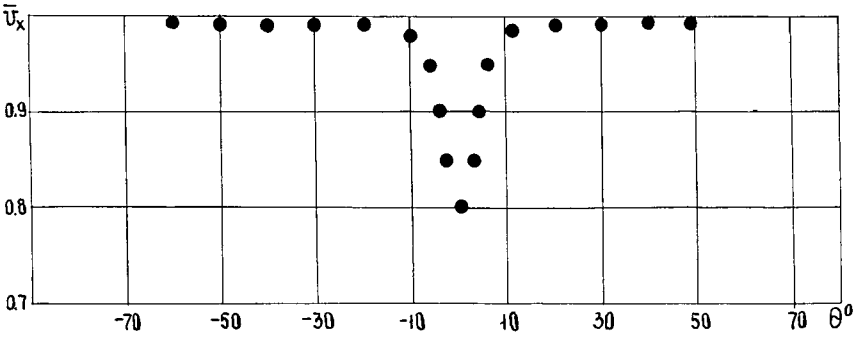

Fig. 14 Results of axial velocity component measurements in foil wake

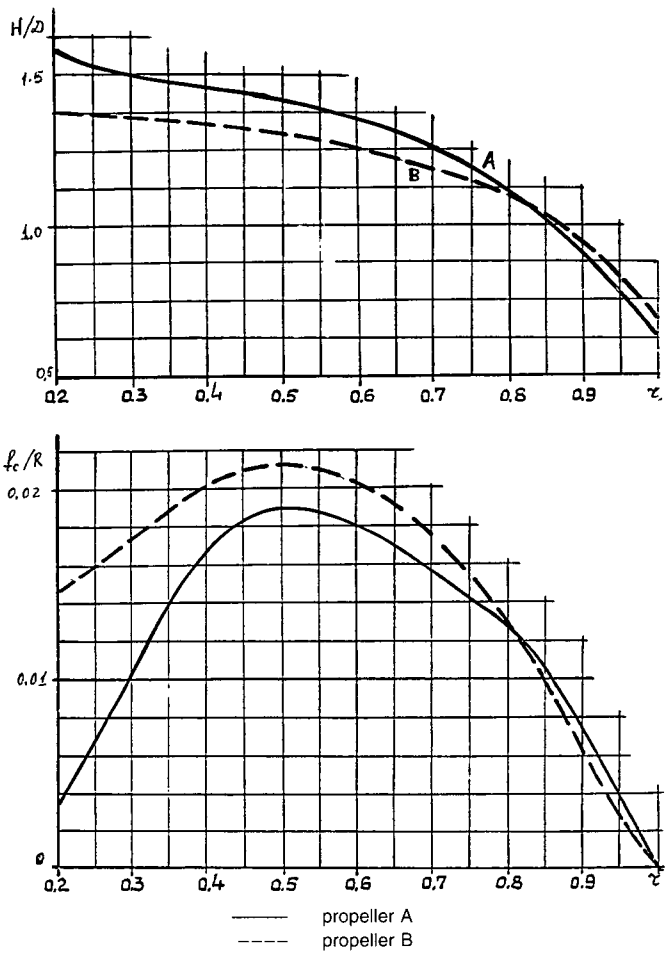

Fig. 15 Geometric characteristics of two blades

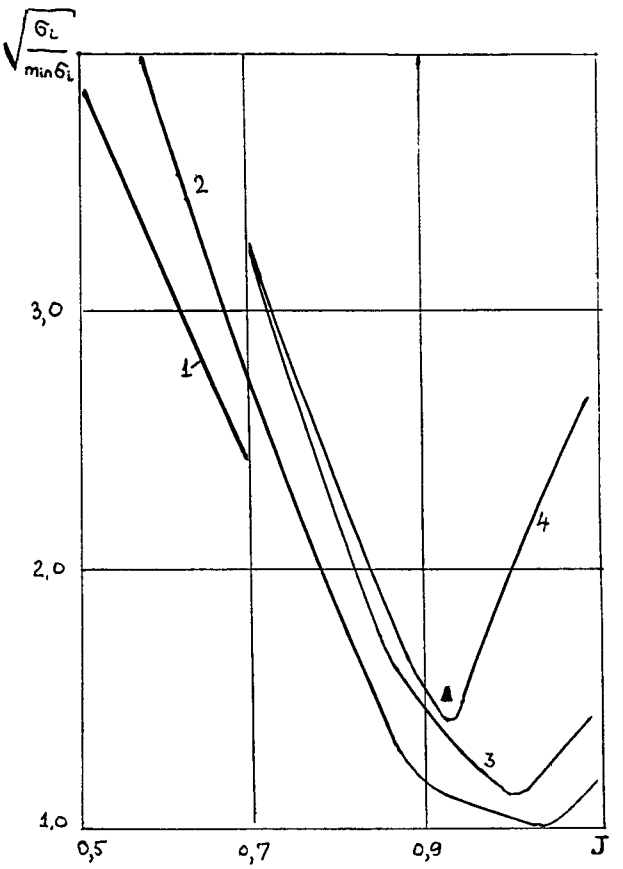

1. ideal flow calculations
2. full-scale uniform flow calculations
3. quasi-steady scaling from model to full-scale
4. unsteady calculation for full-scale conditions
▲ full-scale experimental point

Fig. 16 Propeller cavitation diagram

For the propeller with optimum (according to Betz) circulation distributions the displacement of the left branch of the diagram due to the nonuniform flow distribution was less than in the case of quasi-steady predictions but correlated with the change in thrust coefficient. The model with the unloaded blade tips did not respond to the narrow peak of wake distribution (Figs. 18,19).

Therefore, it may be concluded that the quasi-steady concept is not applicable for predicting tip vortex cavitation on unloaded-tip propeller blades. The physics of this phenomenon may be explained by specific features of tip vortex formation inherent in such propellers. With a Betz-optimum propeller an intensive tip vortex forms due to the stream around the tip edge caused by the high-circulation gradient in this area. On a propeller with unloaded tips the tip vortex appears because the vortex sheet is rolled up in the flow behind the blade. This was confirmed by observations during cavitation tunnel tests: the first bursts of cavitation appeared not on the blades but at a distance downstream from them and this distance was larger than would be necessary to absorb air bubbles into the vortex core in the case of gaseous cavitation.

On blade geometry numerical optimization

The lack of tip-vortex cavitation under full-scale conditions has forced the authors to reconsider blade geometry optimi-

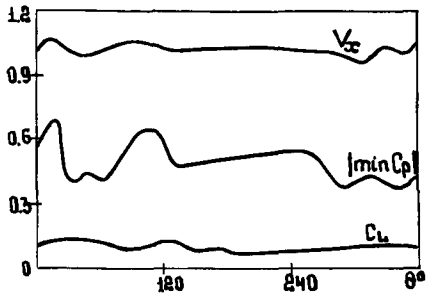

Fig. 17 Typical dependence of hydrodynamic characteristics of blade section at $r = 0.7$ on angle θ

zation principles and ways for further improvement of propeller performance cavitation-wise. Special attention was paid to the design of blade section profiles. A method offered by Alexandrov (1980) and producing results similar to the results of Eppler & Shen (1979) has become widely used at the Krylov Institute. It was also realized that the radius-wise circulation distribution should be selected so as to ensure a uniform distribution of minCp because superfluous tip unloading led to early cavitation inception at $r = 0.5$–0.8 radii. Moderately skewed blades have shown themselves to be an efficient way to delay cavitation inception.

Assuming that the engine parameters (power,rpm), hull resistance, propeller-hull interaction coefficients, wake distribution in the propeller disk, and propeller diameter are known, the task is to design the blade section profiles while the blade-area ratio and hence the blade breadth are chosen so as to prevent the second stage of cavitation; blade thickness is dictated by stress analysis. The most difficult task is to correctly select a pair $\{Kt,J\}$ for the fixed hydrodynamic diagram such that optimum distributions of pitch and maximum camber along the radius would be achieved, providing for as low σ_i as possible. And here the choice of optimum design conditions turns out to be inseparable from the σ_i prediction technique involved.

It has been emphasized already that the semi-empirical method of critical cavitation number prediction is not applicable for the propellers with unloaded blade tips. Still, there remains another problem: How good are the design optimizations based on this method? It may be considered that the design condition optimization is properly grounded so long as the centers of the cavitation diagrams from both the model and full-scale results come to the same point in spite of the difference in the cavitation forms.

In reality however, (see Fig. 12), one may note a sizable shift of this center in the case of the sheet cavitation towards the larger advance ratios compared with the vortex cavitation. Therefore, the propellers optimized in order to remove cavitation inception based on model tests turn out to be not quite optimal in full scale.

A special project involving two propellers was staged to evaluate the possibilities of reducing further the cavitation inception number through blade geometry optimization by computation. The first propeller (A) was optimized based on data from testing 200-mm and 300-mm-diameter models; the second propeller (B)—on the basis of numerical full-scale predictions. Both propellers were designed to achieve the same hydrodynamic performance and had the same diameter (3.74 m), blade planes, and section profiles.

Propeller A was designed for $K_\tau = 0.165$ at $J = 0.91$, propeller B for $K_\tau = 0.18$ at $J = 0.86$. The geometry is shown in Fig. 15; the section profile is described in Table 2. Full-scale observations revealed that the use of a more adequate theory has allowed design of a propeller with a 20% lesser critical cavitation number. As already mentioned, the computed results were also in good agreement with the observations in respect to cavity location. In particular, the following numerical predictions were confirmed. The cavities appeared simultaneously everywhere along the radius, except for the blade tips at $r > 0.8$. There were practically no short-length cavities; with the speed increase the cavity length practically immediately grew to 8% to 10% of the blade chord (see full-scale cavity drawings in Figs. 20,21).

Therefore, it was confirmed that the developed method was applicable for computing full-scale cavitation numbers with the aim of blade geometry optimization.

Conclusions

The recent review of cavitation inception research published by Rode (1991) threw a new light upon this complex phenomenon and all varieties of its manifestation in model tests. The author of that review has made a pessimistic comment that a successful computation of σ_i can result only after long years of detailed calculations of phase transition and

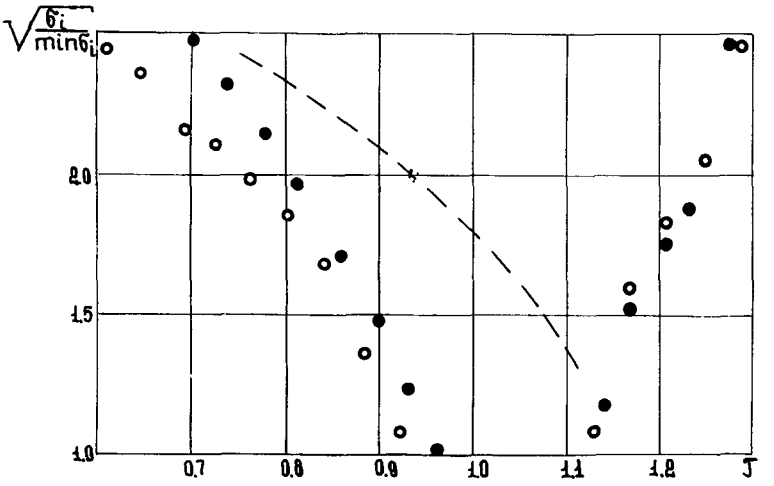

Fig. 18 Measurement results for a propeller model of optimal efficiency

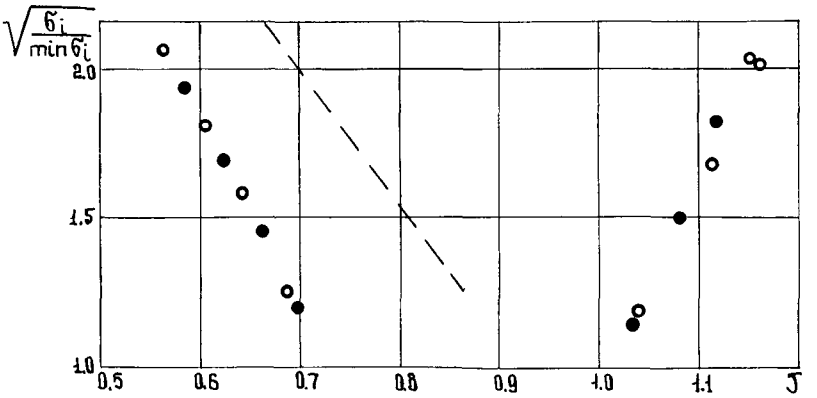

Fig. 19 Measured σ_i of a propeller model with unloaded tip sections; legend corresponds to Fig. 4

Table 2 Reduced blade section parameters

$2x/C$	t/t_{max}	f/f_{max}
−1	0	0
−0.95	0.147	0.081
−0.9	0.226	0.166
−0.8	0.371	0.352
−0.6	0.613	0.691
−0.4	0.799	0.881
−0.2	0.923	0.973
0	0.989	1.0
0.122	1.0	0.988
0.2	0.994	0.97
0.4	0.941	0.881
0.6	0.826	0.731
0.8	0.632	0.506
0.9	0.483	0.343
0.95	0.384	0.248
0.975	0.284	0.167
0.99	0.1634	0.08
1	0	0

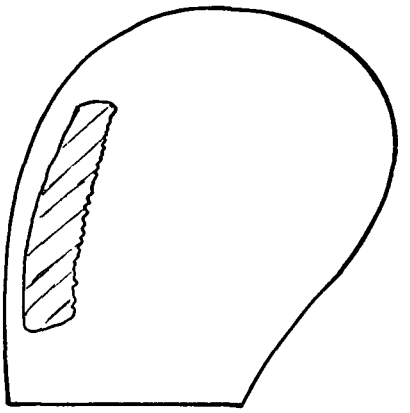

Fig. 20 Cavitation inception pattern on full-scale propeller A; $\sigma = 0.16$

large-scale turbulent structures. The authors of the present report do not expect fast and easy success in finding any sort of a universal theory; it is enough to read Briançon-Marjollet et al (1990) to see the stunning variety of cavitation forms on the same wing tested in one and the same cavitation tunnel. However, the present report once again demonstrates that some of the major values required for routine engineering can be numerically predicted without the knowledge of certain details even for unsteady processes.

It should be also explained why the authors have ignored

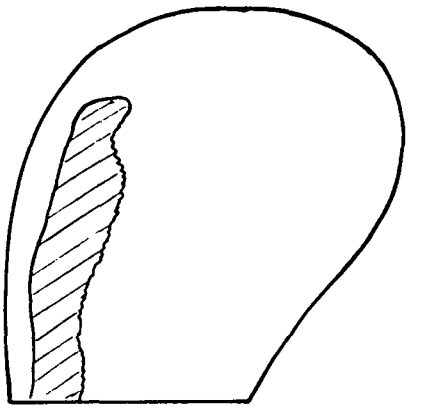

Fig. 21 Cavitation inception pattern on full-scale propeller B; $\sigma = 0.13$

in their computations the gas content, the nuclei content, etc. Of course the authors are aware of the effects which can be caused by a high nuclei content upon cavitation inception in tunnel tests. The point is that at ram values in the stream around the full-scale blades the σ-number is very close to the Euler number even for the gaseous cavitation. That is why the dispersion of the random process of cavitation inception turns out to be so much smaller than σ_i that it is actually lost among other errors.

Acknowledgments

The authors are grateful to the late I. D. Zheltoukhin and to S. V. Kaprantsev for their assistance in full-scale observations and computations. They also extend their gratitude to Prof. A. N. Ivanov and Prof. G. Y. Stepanov for their long years of encouragement during these studies, and to Mr. V. Semenov for his help in writing the English version of this paper.

References

Alexandrov, K. V. 1980 Calculation and design of cavitating profiles. *Papers of Scientific Society of Shipbuilding Industry,* **332** (in Russian).

Amromin, E. L. 1985 On calculation of cavitation flows in viscous and capillar liquid. *Fluid Dynamics,* **20.**

Amromin, E. L. 1988 A condition of cavitation inception. *Fluid Mechanics,* Soviet Research (*Scripta Technica,* USA), 4.

Amromin, E. L. 1993 Etude numerique des ecoulements cavitants autour corps, avee prise en compte de la viscosite. *Journees Hydrodynamique des Nantes,* **4C,** (in French).

Amromin, E. L., Mishkevitch, V. G., and Rozhdestvensky, K. V. 1990 Approximate calculation of three-dimensional cavitation flowing of propeller blades in viscous capillar liquid. *Fluid Dynamics,* **25.**

AMROMIN, E. L., VASILIEV, A. V., AND DROBLENKOV, V. V. 1988 About the different approximation in cavitation flow theory for viscous capillar liquid. *Journal of Appl. Mech., Tech. Phys.,* **29,** 6.

AMROMIN, E. L., VASILIEV, A. V., AND SEMIONITCHEVA, E. YA. 1991 The problems of design of profile with minimal critical cavitation number. *Journal of Appl. Mech., Tech. Phys.,* **32,** 5.

AMROMIN, E. L., VASILIEV, A. V., AND SYRKIN, E. N. 1993 About calculation of critical cavitation number of propellers with taking in consideration of unsteady character of flow. *Fluid Dynamics,* **28.**

ARAKERI, V. H. 1975 Viscous effects of the position of cavitation separation from smooth bodies. *Journal of Fluid Mechanics,* **68,** 4.

ARAKERI, V. H. AND ACOSTA, A. J. 1976 Cavitation inception observation on axisymmetric bodies of supercritical Reynolds numbers. JOURNAL OF SHIP RESEARCH, **20,** 1, March.

BAVIN, V. F., ZAVADOVSKY, N. YU., LEVKOVSKY, YU. L., AND MISHKEVITCH, V. G. 1983 *Propellers. Modern Calculation Methods.* Sudostroenie, Leningrad. (in Russian).

BILLET, M. L. AND HOLL, J. W. 1979 Scale effects on various types of limited cavitation. *Journal of Fluids Engineering,* **3.**

BRIANÇON-MARJOLLET, L., FRANC, J. P., AND MICHEL, J. M. 1990 Transient bubbles interacting with an attached cavity and boundary layer. *Journal of Fluid Mechanics,* **218.**

COLE, J. D. 1968 *Perturbation Methods in Applied Mathematics.* Blaisdell Publ. Comp.

EPPLER, R. AND SHEN, T. 1979 Wing section for hydrofoils—part 1: symmetrical profiles. JOURNAL OF SHIP RESEARCH, **23,** 3, Sept.

GOGISH, L.V. AND STEPANOV, G. YU. 1982 Turbulent separating flows. *Fluid Dynamics,* **17.**

GORSHKOV, A. S. AND KHALASHNIKOV, YU. N. 1970 The scale effect of incipient stage of cavitation on body of revolution. Paper of the Krylov Research Institute, Leningrad, N258 (in Russian).

GREELY, D. AND KERWIN, J. 1982 Numerical methods for propeller design and analysis in steady flow. *Trans.* SNAME, **90.**

HUANG, T. AND PETERSON, F. 1976 Influence of viscous effects on model/full scale cavitation scaling. JOURNAL OF SHIP RESEARCH, **20,** 4, Dec.

IVANOV, A. N. 1980 *Hydrodynamics of Developed Cavitation Flow.* Sudostroenie, Leningrad (in Russian).

KNAPP, R. I., DAILY, J. M., AND HAMMITT, F. G. 1970 *Cavitation.* McGraw-Hill, New York.

KUIPER, G. 1981 Cavitation inception on ship propeller models. Netherlands Ship Model Basin, Wageningen.

LORBER, F. AND COVERT, E. E. 1982 On unsteady airfoil pressure produced by periodic aerodynamic interference. *AIAA Journal,* 9.

NEWMAN, J. N. 1977 *Marine Hydrodynamics.* MIT Press, Cambridge, Mass.

ROOD, E. P. 1991 Mechanisms of cavitation inception. *Journal of Fluids Engineering,* 2.

TULIN, M. P. AND HSU, C. C. 1980 New application of cavity flow theory. *Proceedings,* 13th Symposium on Naval Hydrodynamics, Tokyo.

VAN MEULEN, J. H. J. 1980 Boundary layer and cavitation studies of NACA-16012 and NACA-4412 hydrofoils. *Proceedings,* 13th Symposium on Naval Hydrodynamics, Tokyo.

YAMAGUCHI, H. AND KATO, H. 1983 Nonlinear theory of partially cavitating hydrofoil. *Journal of the Society of Naval Architects of Japan,* **152.**

YAMAGUCHI, H., KATO, H., MAEDE, M., AND MIYANADA, M. 1983 Measurement of pressure distribution in its wake. *Journal of the Society of Naval Architects of Japan,* **152.**